Meteorologische Zeitschrift, Vol. **10**, No. 3, 179-186 (June 2001)

Article

Spectral variation of the solar radiation during an eclipse

PETER KOEPKE*, JOACHIM REUDER and JAN SCHWEEN

Universität München, Germany

(Manuscript received May 31, 2000; in revised form November 3, 2000; accepted November 3, 2000)

Abstract

The time dependent variation of the spectral extraterrestrial solar flux is modelled for the conditions during a total eclipse. These data are used to calculate irradiance and actinic flux at the Earth's surface for atmospheric conditions of August 11, 1999 at Weihenstephan. These results are compared with measurements. It is shown, that the spectral composition of solar radiation varies during the eclipse, since solar limb darkening has a spectral dependence. The solar radiation differs from that of a hypothetical sun without limb darkening by up to 30% in the near IR at 1500 nm and 60% in the UV-B at 310 nm. As shown by a comparison of modelling and measurements, this spectral variation has to be taken into account for modelling of UV radiative quantities in the atmosphere and resulting photochemical processes. The effect of broken cloudiness on irradiance and actinic flux and its dependency on wavelength and receiver geometry is explained.

Zusammenfassung

Der Verlauf der spektralen extraterrestrischen solaren Strahlung während einer Sonnenfinsternis wurde berechnet. Basierend auf diesen Daten, unter Berücksichtigung der atmosphärischen Bedingungen am 11. August 1999 in Weihenstephan, wurden Globalstrahlung und Aktinischer Fluss am Boden modelliert und mit Messwerten verglichen. Die spektrale Zusammensetzung der Strahlung ändert sich während einer Sonnenfinsternis, bedingt durch die wellenlängenabhängige Randverdunklung der Sonne. Im Vergleich zu einer hypothetischen Sonne ohne Randverdunklung ist die solare Strahlung im nahen IR um bis zu 30% gemindert und im UVB bei 310 nm um bis zu 60%. Diese spektralen Änderungen sollten bei der Modellierung von Strahlung, z.B. für photochemische Prozesse berücksichtigt werden. Dies wurde durch Messung und Modellierung gezeigt. Der Einfluss von Wolken auf gemessene Werte von Globalstrahlung und Aktinischem Fluss wurde untersucht und erklärt.

1 Introduction

The knowledge of the spectral behaviour of solar radiation at the Earth's surface is necessary to address many questions in the earth and atmospheric sciences. The spectral behaviour can be measured and modelled. Modelling provides data for times and places without actual measurements and has the advantage of giving irradiance and actinic flux simultaneously. To determine solar radiation quantities at the Earth's surface, the extraterrestrial solar radiation is used to illuminate the atmosphere, for which the scattering and absorption processes are spectrally modelled. In general the extraterrestrial solar irradiance at each wavelength is given as an average over the whole solar disc. During different times of an eclipse, the disk of the moon covers different parts of the limb and the center of the sun. Thus the spectral dependence of the limb darkening of the sun becomes relevant.

Measurements of radiative quantities have been made during earlier eclipse events (KIMBALL and FERGUSSON, 1919; JERLOV et al., 1954; BELETSKY et al., 1997). During previous eclipse events a point of interest was the derivation of total ozone content from UV radiation measurements (STRANZ, 1961; OSHEROVICH et al., 1974; CHAKRABARTY et al., 1997). It was realised that the spectral dependence of solar limb darkening plays an important role, especially when the total ozone content is measured using spectrophotometers (BOJKOV, 1968; MIMS and MIMS, 1993). Several approaches exist to estimate the effect of limb darkening (SVENSSON, 1958; HUNT, 1965; OUTCALT and MEISEL, 1970). However, due to limitations in computing capacity, the corresponding values have been tabulated only for a few wavelengths and with low temporal resolution.

Improvements in measurement and modelling enable us to make a more detailed investigation of the spectral behaviour of solar radiation during an eclipse. Thus the analysis of actual data is worthwhile, especially because a comparison with model results is possible nowadays. During the eclipse of August 11, 1999, radiation measurements were influenced by variable cloud conditions. The spectral effect of clouds on various radiative quantities depends on cloud amount, position of the clouds relative to the sun and on the receiver geometry (HERMAN and MCKENZIE, 1999). The measurements during

* Corresponding author: Peter Koepke, Meteorologisches Institut der Universität München, Arbeitsgruppe für Strahlung und Satellitenmeteorologie, Theresienstraße 33, 80333 München, Germany, e-mail: Peter.Koepke@lrz.uni-muenchen.de

0941-2948/01/0010-0179 $ 03.60

DOI: 10.1127/0941-2948/2001/0010-0179

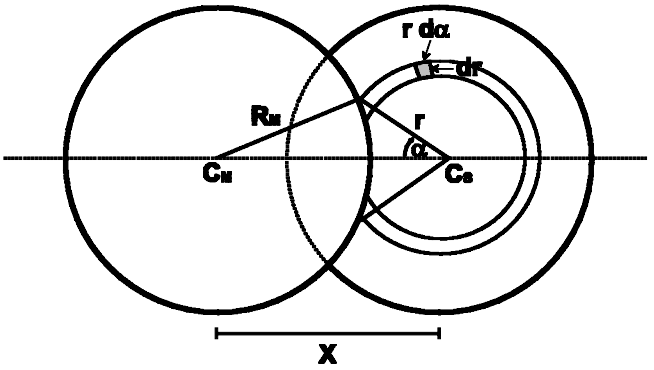

Figure 1: Geometrical relationships for the calculation of the radiation from the visible part of the solar disk during the eclipse.

the eclipse give us the opportunity to separate these different factors.

2 Solar radiation outside the atmosphere

During the eclipse of August 11, 1999, the average diameter of the moon was 31.982', that is about 1.3% larger than that of the sun with 31.560'(U.S. NAVAL OBSERVATORY, 1998).

A consequence of the similar sizes of the apparent disks of sun and moon is that at the beginning of and close to the end of the eclipse the moon covers only parts of the solar limb, while the centre of the sun is uncovered. Close to the total coverage, in the middle of the event, only a small crescent of the sun is visible, an area which is completely part of the solar limb region. Thus the relative contribution of centre and limb to solar irradiance varies during the eclipse. The radiation from the limb of the solar disk is less intense than that from the centre. Moreover this limb darkening is spectrally dependent. Thus the spectral composition of the irradiance of the sun changes during the eclipse.

Based on considerations of the radiative transfer within the solar atmosphere, the limb darkening Γ_λ can be expressed as a function of r, the relative distance from the centre of the solar disk (WALDMEIER, 1941; SCHEFFLER, 1974),

$$\Gamma_\lambda(r) = \frac{I_\lambda(r)}{I_\lambda^0} = \frac{1+\beta_\lambda \cdot \sqrt{1-r^2}}{1+\beta_\lambda} \tag{2.1}$$

where $r = 0$ represents the centre and $r = 1$ the limb of the sun. $I_\lambda^0 = I_\lambda(r=0)$ denotes the intensity coming from the centre of the solar disk.

The so-called limb darkening coefficient β_λ is a function of wavelength (WALDMEIER, 1941):

$$\beta_\lambda = \frac{3 \cdot h \cdot c \cdot \sqrt[4]{2}}{8 \cdot k \cdot \lambda \cdot T_S} \tag{2.2}$$

where λ is wavelength in m, h the PLANCK constant ($6.63 \cdot 10^{-34}$ J s), c the speed of light ($2.998 \cdot 10^8$ m s^{-1}), k the Boltzmann constant ($1.38 \cdot 10^{-23}$ J K^{-1}) and T_S the temperature of the sun's surface (5740 K).

Using $\Gamma_\lambda(r)$ given in Eqn. 2.1, the spectral irradiance of the uncovered sun can be calculated by integrating over the whole solar disk:

$$I_{S\lambda} = \int_0^{R_S}\int_0^{2\pi} I_\lambda^0 \cdot \Gamma_\lambda(r) \cdot r\, d\alpha\, dr = 2\pi \cdot I_\lambda^0 \cdot \int_0^{R_S} \Gamma_\lambda(r) \cdot r\, dr \tag{2.3}$$

During the eclipse, part of the solar disk is covered by the moon leading to a reduced solar intensity $I_{C\lambda}$. The geometrical relationships for the mathematical description of this problem are sketched in Fig. 1. The distance between the centres of the disks of the moon (C_M) and the sun (C_S) is denoted as X, which is normalised by its value at the moment of the first contact, where the distance equals the sum of the radii of moon and sun, $R_M + R_S$. The value of X is linearly correlated to time. Due to the slightly larger apparent radius of the moon, totality occurs for $0.0064 \geq X \geq -0.0064$. The value of $X = -1$ defines the time at which the disk of the moon leaves the sun again. When $X > R_M$ and $r \leq X - R_M$ the angular integration is performed over a complete circle. When $X < R_M$ and $r \leq R_M - X$ the annulus is behind the disk of the moon and omitted from integration. For $r > |X - R_M|$ a sector with an angle 2α will not contribute to the radiation and will be excluded from integration. This angle α can be determined from geometrical considerations as a function of X and r:

$$\alpha(r,X) = \begin{cases} 0 & \text{if } X - R_M \geq r \text{ and } X > R_M \\ \arccos\left[\frac{r^2+X^2-R_M^2}{2 \cdot r \cdot X}\right] & \text{if } |X - R_M| < r \\ \pi & \text{if } R_M - X > r \text{ and } X \leq R_M \end{cases} \tag{2.4}$$

The integration of the irradiance from the remaining solar disk not covered by the moon thus becomes:

$$\begin{aligned} I_{C\lambda} &= \int_0^{R_S}\int_\alpha^{2\pi-\alpha} I_\lambda^0 \cdot \Gamma_\lambda(r) \cdot r\, d\alpha\, dr \\ &= 2\pi \cdot I_\lambda^0 \cdot \int_0^{R_S} \left[1 - \frac{\alpha(r,X)}{\pi}\right] \cdot \Gamma_\lambda(r) \cdot r\, dr \end{aligned} \tag{2.5}$$

This equation has been integrated numerically. For a description of the spectral variation of the solar irradiance during eclipse, the normalised irradiance I_{norm}, i.e. the ratio between the irradiance of the remaining part of the sun $I_{C\lambda}$ (Eqn. 2.5) and the irradiance of the uncovered solar disk $I_{S\lambda}$ (Eqn. 2.3), is used:

$$I_{norm,\lambda} = \frac{I_{C\lambda}}{I_{S\lambda}} \tag{2.6}$$

Fig. 2 shows the decrease in $I_{norm,\lambda}$ with decreasing X due to an increase in the area of the sun covered by the moon. The bold grey line represents the normalised intensity of a hypothetical sun without limb darkening, i.e.

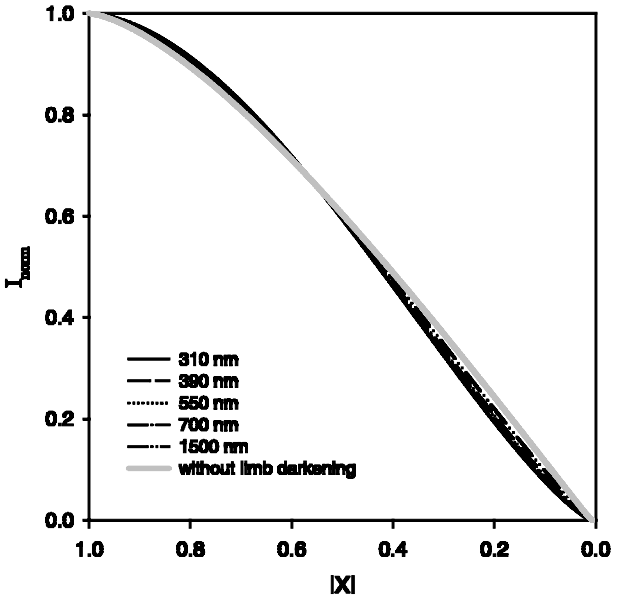

Figure 2: Normalised radiation as function of X, the distance of the centers of moon and sun, during eclipse for different wavelengths.

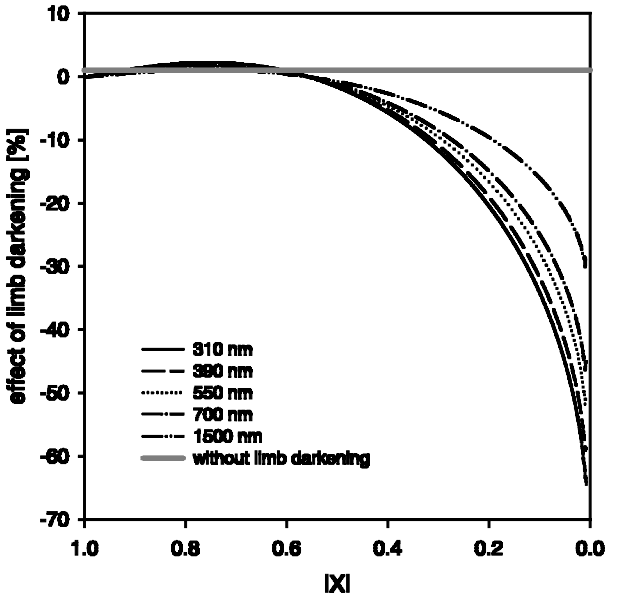

Figure 3: Effect of limb darkening as a function of X for different wavelengths.

$\Gamma(r) = 1$. Due to the wavelength dependence of the limb darkening, $I_{norm,\lambda}$ is wavelength dependent. This effect is shown in Fig. 2 for 5 different wavelengths. These wavelengths are chosen to cover the spectral range of interest. The two wavelengths in the UV spectral region, 310 nm and 390 nm, are important for the description of the photochemical processes of ozone and nitrogen dioxide photolysis discussed in the paper by FABIAN et al. in this issue. The wavelength 550 nm is given as a standard wavelength for visible light and 700 nm is very close to the solar median-wavelength, which divides the solar irradiance energetically into two equal parts and is therefore useful to describe the average behaviour of the integrated solar irradiance. Finally, 1500 nm is shown as an example for a wavelength of the infrared spectral range. Compared to the hypothetical case without limb darkening $I_{norm,\lambda}$ is enhanced for $|X| > 0.55$, at the beginning and the end of the eclipse. At that time mainly parts of the darker limb are covered, while the brighter central region of the sun contributes fully. During the central part of the eclipse ($|X| < 0.55$) $I_{norm,\lambda}$ is reduced, because most of the radiation comes from the limb region, while the centre of the sun is covered by the moon. The resulting spectral behaviour agrees well with tabulated values given by OUTCALT and MEISEL (1970). However, they give values for a few selected wavelengths only and do not give equations, which would allow further calculations.

Fig. 3 displays the spectral dependence of the solar radiation during the eclipse in detail as percentage deviation from a sun without limb darkening. Since the radiation at shorter wavelengths shows a stronger limb darkening effect, it is less strongly reduced at the beginning and more strongly reduced close to the central part of the eclipse. The reduction of the radiation at longer wavelengths is more uniform over the whole period. The enhancement reaches its maximum of 2.5% in the UV and of about 1% in the infrared at $|X| = 0.75$. This maximum occurs when about 15% of the sun is covered by the moon. As totality is approached, the effect of limb darkening becomes more and more important, and $I_{norm,\lambda}$ is reduced by about 30% at 1500 nm and by more than 60% at 310 nm. The effect of limb darkening has to be taken into account especially in the photochemically relevant UV spectral range. In this spectral region a reduction of 10% is reached for $|X| = 0.35$, when 40% of the sun is uncovered. At $|X| = 0.2$, when more than 25% of the sun is still visible, $I_{norm,\lambda}$ is reduced by 20%.

3 Solar radiation at the surface

3.1 Model calculations

Model calculations have been carried out for both eclipse and non-eclipse conditions to obtain the variation of various radiative quantities during the eclipse, under real atmospheric conditions but without the influence of clouds. The simulations of the radiative processes in the atmosphere have been performed by an improved version of the radiative transfer model STAR (RUGGABER et al. 1994; SCHWANDER et al., 2000). It is based on a one-dimensional radiative transfer algorithm (NAKAJIMA and TANAKA, 1988) that considers absorption and scattering (including multiple scattering) of air molecules, aerosol particles and atmospheric trace gases. To calculate solar radiation for August 11, 1999 the actual atmospheric conditions have been taken into account. While the solar zenith angle is changed in the model runs, the state of the atmosphere is assumed to be unchanged during the eclipse.

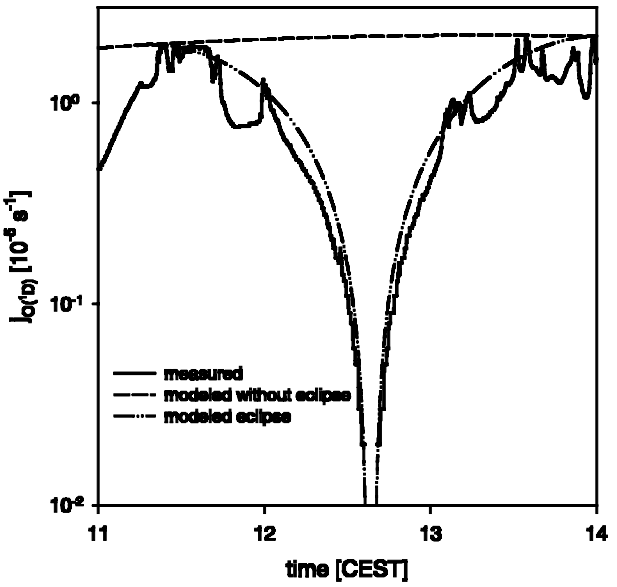

Figure 4: Measurements and model calculations of ozone photolysis frequency $j_{O(^1D)}$ at WHS.

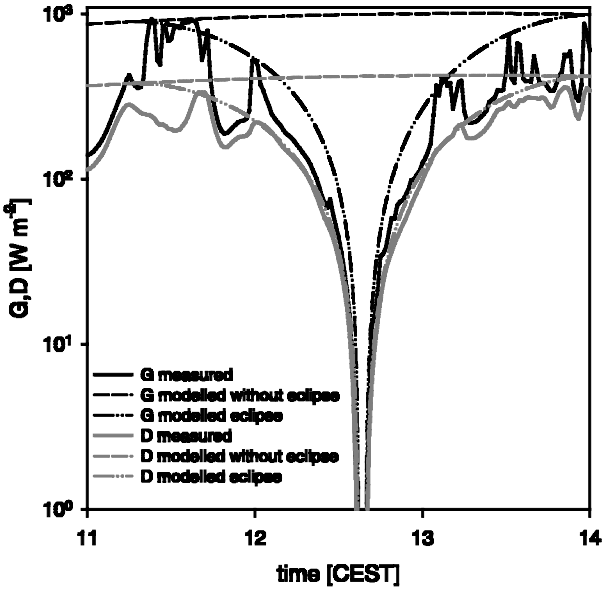

Figure 5: Measurements and model calculations of total solar irradiance G and diffuse solar irradince D at WHS.

The total ozone content (318 DU) results from BREWER measurements performed at the Meteorological Observatory Hohenpeißenberg (KÖHLER et al., 1998) about 100 km south-west of Weihenstephan (WHS) and additional total ozone measurements using a Microtops device at Kaltenberg about 85 km south-west of WHS. The aerosol description has been compiled on the basis of visibility observations and an air mass analysis, resulting in the low absorbing aerosol type 'clean continental' from the OPAC database (HESS et al., 1998). From visibility observations (around 50 km) in combination with the assumptions of the aerosol height distribution used by STAR, the aerosol optical depth (AOD) at 550 nm was deduced to be 0.2. The spectral behaviour of the selected aerosol type results in an AOD of 0.4 in the UV-B region around 310 nm. The surface was chosen to be a mixture of concrete and vegetation in accordance to the situation at the measurement sites. Model calculations were performed for cloud-free conditions.

Based on these atmospheric properties, photolysis frequencies $j_{O(^1D)}$ and j_{NO_2}, the integral UV irradiance G_{UV}, the irradiance at 310 nm G_{310}, and the total solar irradiance and its diffuse and direct components at 700 nm were modelled by STAR for non-eclipse conditions. These calculations are based on the actual sun-earth distance and solar zenith angles. To model the variation during the eclipse, the various radiative quantities resulting from STAR have been multiplied by the factor $I_{norm,\lambda}$ (Eqn. 2.6). This can be done because the optical properties of the atmosphere are independent of the intensity of radiation incident at the top of the atmosphere. For this calculation the influence of scattered radiation with different spectral composition from regions outside the path of the total eclipse is neglected. This assumption is valid because the vertical extension of the atmosphere is much smaller than the horizontal dimension of the umbral shadow.

3.2 Radiation measurements

During the eclipse of August 11, 1999 a wide range of solar radiation measurements were made at WHS (FABIAN et al., this issue, 2001a). The measurements enclose the solar irradiance integrated over various spectral regions (total solar irradiance G, diffuse sky irradiance D, UV-irradiance G_{UV}) and two photochemically relevant radiative quantities, the photolysis frequencies of ozone ($j_{O(^1D)}$) and nitrogen dioxide (j_{NO_2}). In contrast to the irradiance, which represents the cosine-weighted radiation on a horizontal plane, the latter quantities are based on the actinic flux, and therefore use a detector geometry which detects radiation independent of the incidence angle. A description of the corresponding detectors and the details of the method of photolysis frequency measurement can be found at JUNKERMANN et al. (1989) and REUDER et al. (1996). The accuracy of the method is estimated to be about $\pm$ 10% for j_{NO_2} and $\pm$ 15% for $j_{O(^1D)}$ (MÜLLER, 1994; REUDER, 1999). In addition to the measurements at WHS spectral solar irradiance at a wavelength of 310 nm was monitored during the eclipse at the site Neuherberg (NH), located in a suburban area north of Munich, about 25 km south-west of WHS. These measurements were obtained using a double monochromator system (BENTHAM DM300). Details of the location of both sites are given in Table 1.

Figs. 4 and 5 show measurements and model calculations of different radiative quantities for non-eclipse and eclipse conditions at WHS and Fig. 6 shows G_{310} at NH, all from 11:00 to 14:00 CEST (Central European Summer Time). It can be seen that the measurements performed at WHS indicate a distinct influence

Table 1: Site information and time schedule for the eclipse of August 11, 1999 at Neuherberg (48.2214°N, 11.5883°E, 493 m a.s.l.) and Weihenstephan (48.4014°N, 11.7194°E, 498 m a.s.l.).

Contact no.	*Description*	*X*	*Neuherberg (NH)*	*Weihenstephan (WHS)*
1	moon enters solar disk	1	11:16:25	11:16:41
2	begin of totality	0.064	12:37:09	12:37:19
3	end of totality	–0.064	12:39:25	12:39:35
4	moon leaves solar disk	–1	14:01:22	14:01:24

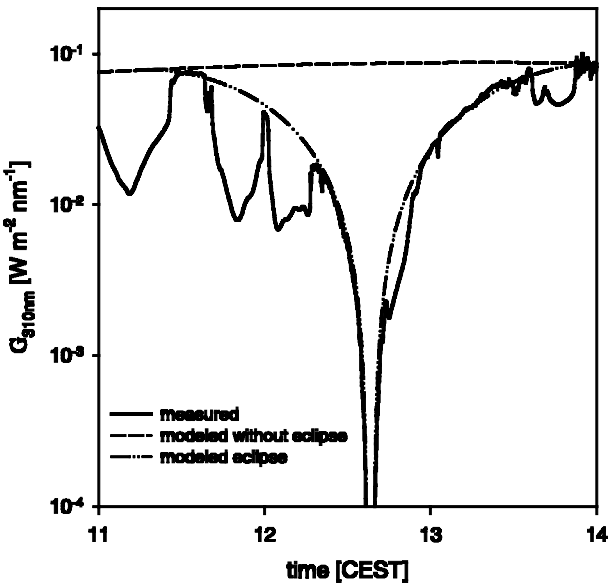

Figure 6: Measurements and model calculations of spectral irradiance at 310 nm G_{310} at NH.

of clouds during the eclipse. Except for the time around 11:30 CEST close to the beginning of the eclipse, when a larger cloud gap provided radiative conditions widely undisturbed by clouds for nearly half an hour, the whole period under investigation is influenced by clouds. As a consequence, the measured values are below those from the cloud-free simulations for most of the time. After 12:00 CEST the measured values reach the modelled ones, but only for a few minutes. Ozone photolysis frequency (Fig. 4) and nitrogen dioxide photolysis frequency (not shown), even sometimes are enhanced above the corresponding cloud-free simulations. This is a well-known phenomenon in a cloudy atmosphere with cloud cover between 5 and 7 octas (e.g. REUDER, 1999) and also may occur in irradiance. In situations when the direct solar beam is not shaded by a cloud the additional reflection of solar radiation from vertically extended clouds (especially cumulus) can increase the incoming radiation at the detector by up to 25% above the corresponding cloud-free values.

Fig. 5 shows the solar global irradiance G and its diffuse component D. Due to the spectral limitation of STAR to wavelengths between 280 nm and 700 nm, an absolute determination of total solar irradiance, including the near-infrared range up to 3 μm, cannot be done directly. Therefore the simulations of G and D are based on the spectral total irradiance at 700 nm, a wavelength close to the solar median-wavelength (CIE, 1989) which can be assumed to be representative of the solar spectral range. The agreement between measured and modelled values of D between 12:00 and 13:00 CEST indicates that the effect of the eclipse, including the spectral dependent limb darkening, is considered correctly. D is the appropriate quantity to prove this agreement between cloud-free model calculations and measurements in the presence of clouds. Due to the fact that the direct component of the solar radiation is continuously shaded by the shadow-band, the values of D are nearly insensitive to the shading of the direct solar beam by clouds. As long as the average distribution of the clouds at the sky remains similar, there are only minor cloud effects on D. Only in situations where large areas of the sky are covered by thick clouds, as can be seen before 12:00 CEST and after 13:15 CEST, is D markedly reduced. The cloud influence close to totality is weaker at the site NH than at WHS (see the RADAR image given by WINKLER et al., this issue, 2001). Consequently the measured values of G_{310} (Fig. 6) agree well with the simulations also between 12:15 and 12:45 CEST.

3.3 Hypothetical non-eclipse radiation

To investigate the effect of the eclipse on photochemistry, especially on the concentrations of relevant atmospheric trace gases, corresponding measurements and box model calculations have been performed (FABIAN et al., this issue, 2001b). The model run 'eclipse' was photochemically driven by photolysis frequencies directly measured during the eclipse (e.g. Fig. 4). A control model run under non-eclipse conditions has been performed to quantify the influence of the eclipse. For this purpose a second photolysis frequency data set has been compiled, which represents the radiative conditions of August 11 under the actual atmospheric conditions, including cloud influence, but without the eclipse. Based on the photolysis frequencies, j_e, measured during the eclipse, and the normalised radiation, $I_{norm,\lambda}$, (Eq. 2.6) derived from model calculations, photolysis frequencies, j_{ne}, under the assumption of non-eclipse conditions have been determined by:

$$j_{ne} = \frac{j_e}{I_{norm,\lambda}} \tag{3.1}$$

The normalised radiation at a wavelength of 310 nm has been used to compensate for the effect of the eclipse on $j_{O(^1D)}$. The correction of j_{NO_2} has been done at the wavelength of 390 nm. The resulting data sets of $j_{O(^1D)}$ and j_{NO_2} have similar relative variation with time and therefore again only $j_{O(^1D)}$ is plotted (Fig. 7). The uncertainty in j_{ne} is high during about 15 minutes centered around totality, due to both low and thus uncertain values of measured photolysis frequencies, and values of I_{norm} close to zero. Therefore all data points in the central part of Fig. 7 with an error in excess of 30% derived by Gaussian error propagation, were replaced by the constant values of $1.52 \cdot 10^{-5}$ s^{-1} for $j_{O(^1D)}$ and $5.2 \cdot 10^{-5}$ s^{-1} for j_{NO_2}. These values represent average conditions for the time intervals before and after totality.

3.4 Effects of clouds and limb darkening on radiation

The measurements presented in the previous sections show that the expected spectral eclipse effect is masked by cloud effects to a great extent. In the following, both effects will be separated as far as possible by a detailed analysis of the measurements.

The main effect of clouds is the blocking of the direct solar beam, resulting in local shadow. Although there are some indications that cloud transmittance itself is weakly wavelength dependent (e.g. SECKMEYER et al., 1996; THIEL, 1999), this must not be taken into account for situations with scattered clouds. In this case the contribution of the photons transmitted through the clouds is negligible. In the case of broken cloudiness, the spectral effects on radiation reaching the ground are mainly caused by the strong wavelength dependence of the ratio of diffuse and direct radiation. The larger the contribution of diffuse radiation to a measured radiative quantity, the less will be the influence of such a cloud effect. To quantify these effects in general, the distribution of diffuse and direct radiation was calculated by STAR for conditions representing an average cloudless state of the atmosphere at WHS during the eclipse (see section 3.1). The calculations have been performed for both, irradiance and actinic flux, and for different wavelengths. The resulting portion of the direct component is given in Table 2. Irradiance as well as actinic flux show a distinct increase of the relative contribution of the direct component toward longer wavelengths. Scattering processes involving air molecules and aerosol particles convert direct solar radiation into diffuse radiation. Due to the increased efficiency of scattering processes with decreasing wavelength, diffuse radiation becomes more and more important at shorter wavelengths at the Earth's surface. As a consequence, the direct component of the irradiance decreases from 85% at 700 nm to 37% at 310 nm at noon on August 11 (solar zenith angle: 33°; total ozone: 318 DU; aerosol type: clean continental; AOD at 550 nm: 0.2). The corresponding values for the actinic flux, relevant for photolysis frequencies, decrease from 74% to 26%. Due to the missing cosine-weighting in the actinic flux, the diffuse radiation far from the zenith contributes more strongly to the signal. Therefore the relative contribution of the direct component in the actinic flux is systematically lower than in the irradiance. Thus the irradiance will be more strongly reduced than the actinic flux when the sun is obscured by a cloud.

Table 2: Relative contribution of the direct radiation component to irradiance and actinic flux for different wavelengths. The values are based on STAR calculations using actual atmospheric parameters at WHS on August 11, 1999, assuming cloud free conditions.

Wavelength [nm]	*Irradiance*	*actinic flux*
310	37%	26%
390	58%	44%
550	77%	65%
700	85%	74%

Fig. 8 shows a comparison of G, G_{UV}, $j_{O(^1D)}$, and j_{NO_2} measured at WHS. The data are normalised to 1 at 11:38 CEST, because the cloud influence was minimal during a cloud gap episode at that time. The eclipse effect can be neglected at this time shortly after the first contact of the disks of sun and moon. It is evident that the cloud influence increases with increasing wavelength due to the higher portion of direct radiation at longer wavelengths, as mentioned above. This spectral dependence can be seen for both irradiances (G is attenuated stronger than G_{UV}) and the photolysis frequen-

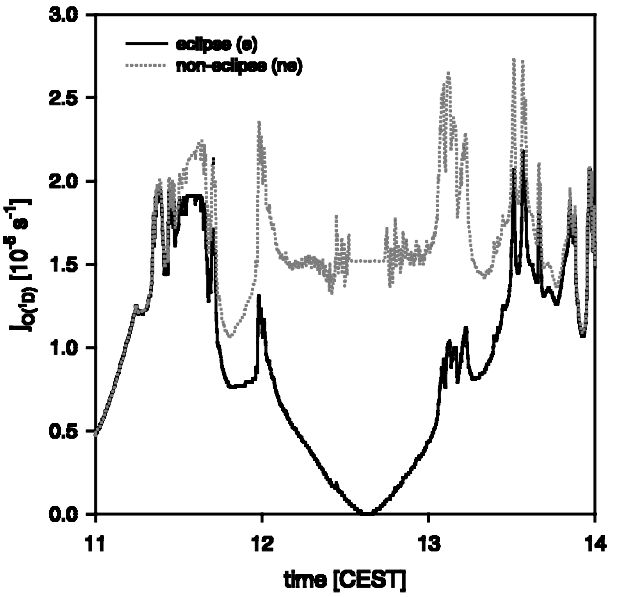

Figure 7: Photolysis frequencies of ozone during eclipse. The solid line gives the measurements, the dotted line represents hypothetical values assuming non-eclipse conditions.

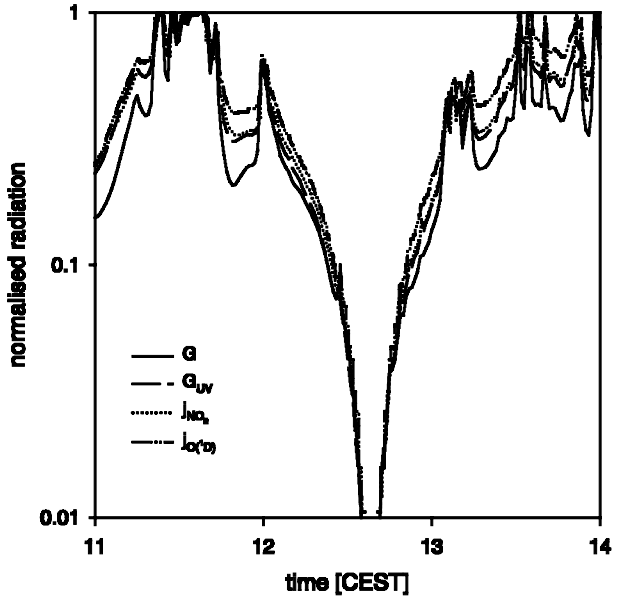

Figure 8: Selected radiation quantities during eclipse. All data are normalised at 11:38, a situation with minimum cloud impact.

cies based on the actinic flux (j_{NO_2} is attenuated stronger than $j_{O(^1D)}$). Within a similar spectral range, 290 nm to 420 nm with a maximum sensitivity around 390 nm for j_{NO_2} and 295 nm to 385 nm for the Eppley radiometer used for the measurement of G_{UV}, the cloud effect is more pronounced in the case of the irradiance G_{UV}. Again this is caused by the higher portion of direct radiation in the case of G_{UV} (58% compared to 44% for the actinic flux at 390 nm, see Table 2).

For a better visualisation of the effects close to totality and for a quantification of the effects during the whole eclipse, the ratios of G_{UV}/G and $j_{O(^1D)}/j_{NO_2}$ calculated from normalised values have been plotted in Fig. 9. Ratios larger than 1 indicate that the quantity in the numerator (here in each case the quantity determined at shorter wavelengths) is less attenuated than the quantity in the denominator. During episodes where the sun is obscured by clouds, the ratios reach values of 1.4 to 1.6 for G_{UV}/G and 1.1 to 1.2 for $j_{O(^1D)}/j_{NO_2}$. As discussed in detail above, this difference is caused by the variable portion of the direct radiation component for the spectral intervals involved.

The spectral effect of limb darkening during the eclipse can be seen in the ratio G_{UV}/G. Although modified by the cloud effects, it shows a distinct decrease toward totality, reaching values below 0.85. In contrast to the cloud effect, the spectral effect of limb darkening increases with decreasing wavelength (see Fig. 3). The more of the sun is covered by the moon during eclipse, the stronger the limb darkening effect. Close to totality it is even strong enough to overcompensate the cloud influence, leading to values of the ratio G_{UV}/G below 1. In contrast, there is no obvious effect of limb darkening visible in the ratio $j_{O(^1D)}/j_{NO_2}$, because the relevant wavelength intervals of $j_{O(^1D)}$ and j_{NO_2} are too close to each other.

4 Conclusion

Solar radiation during the eclipse of August 11, 1999 has been measured and modelled. To describe the spectral behaviour of solar radiation outside the atmosphere an equation was derived for the important effect of limb darkening. When compared to a sun without limb darkening this effect reaches maximum values of 30% at 1500 nm and more than 60% at 310 nm. This result indicates that this effect has to be taken into account for investigations of radiative effects, especially in the photochemically relevant UV spectral range.

The extraterrestrial radiation resulting from the limb darkening calculations has been used as input for the radiative transfer model STAR. Model results, using actual atmospheric parameters, show a good agreement with measurements for various radiative quantities. This indicates the quality of both the modeled extraterrestrial and atmospheric effects and the measurements.

Clouds in front of the sun also cause a wavelength dependent decrease of irradiance and actinic flux. This can be explained by the spectral dependency and the relative contribution of direct and diffuse radiation. The results support the hypothesis that the actual coverage of the sun by a cloud is the essential information to describe the influence of cloudiness on solar radiation at the Earth's surface. The widely used description cloudiness by cloud cover given in octas provides information less suitable, even if this is available for different cloud layers.

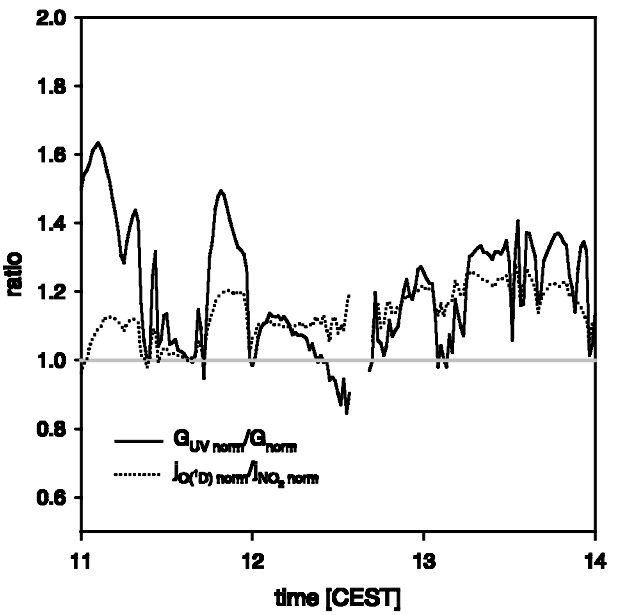

Figure 9: Ratios of normalised irradiances (solid) and normalised actinic fluxes (dotted) during the eclipse.

Acknowledgments

We are grateful to the Bundesamt für Strahlenschutz, Institut für Strahlenhygiene for providing their instrumentation to measure spectral UV radiation at Neuher-

berg, to Deutscher Wetterdienst, Meteorologisches Observatorium Hohenpeißenberg for the provision of total ozone measurements, and to the Technische Universität München, Lehrstuhl für Bioklimatologie und Immisionsforschung for the radiation measurements at Weihenstephan.

References

BELETSKY, A.B., A.V. MIKHALEV, M.A. CHERNIGOVSKAYA, 1998: Spectral measurements of the solar near-ground UV radiation during the solar eclipse on March 9, 1997. – Atmos. Oceanic Opt. **11**, 301–306.

BOJKOV, R.D., 1968: The ozone variations during the solar eclipse of 20 May 1966. – Tellus **20**, 417–421.

CIE, 1989: Solar spectral irradiance. – Publ. **CIE85**, ISBN 3900734224,48 pp.

CHAKRABARTY, D.K., N.C. SHAH, K.V. PANDYA, 1997: Fluctuations in ozone column over Ahmedabad during the solar eclipse of 24 October 1995. – Geophys. Res. Lett. **24**, 3001–3003.

FABIAN, P., M. WINTERHALTER, B. RAPPENGLÜCK, H. REITMAYER, A. STOHL, P. KOEPKE, H. SCHLAGER, H. BERRESHEIM, TH. FOKEN, B. WICHURA, K.-H. HÄBERLE, R. MATYSSEK, TH. KARTSCHALL, 2001a: The BAYSOFI Campaign – Measurements carried out during the total solar eclipse of August 11, 1999. – Meteorol. Z. **10**, 165–170.

FABIAN, P., B. RAPPENGLÜCK, A. STOHL, H. WERNER, M. WINTERHALTER, H. SCHLAGER, P. STOCK, H. BERRESHEIM, U. KAMINSKI, P. KOEPKE, J. REUDER, W. BIRMILI, 2001b: Boundary layer photochemistry during a total solar eclipse. – Meteorol. Z. **10**, 187–192.

HERMAN, J., R.L. MCKENZIE, 1999: Surface Ultraviolet Radiation. – In: Scientific Assessment of Ozone Depletion: 1998, ENNIS, C.A. (Ed.). World Meteorological Organization, Global Ozone Research and Monitoring Project, Geneva, 46 pp.

HESS, M., P. KOEPKE, I. SCHULT, 1998: Optical Properties of Aerosols and Clouds: The Software Package OPAC. – Bull. Am. Meteorol. Soc. **79**, 831–844.

HUNT, B.G., 1965: A theoretical study of the changes occuring in the ozonosphere during a total eclipse of the sun. – Tellus **17**, 516–523.

JERLOV, N., H. OLSSON, W. SCHUEPP, 1954: Measurements of solar radiation at Lövanger in Sweden during the total eclipse 1945. – Tellus **6**, 44–45.

JUNKERMANN, W., U. PLATT, A. VOLZ-THOMAS, 1989: A photoelectric detector for the measurement of photolysis frequencies of ozone and other atmospheric molecules. – J. Atmos. Chem. **8**, 203–227.

KIMBALL, H.H., S.P. FERGUSSON, 1919: Influence of the solar eclipse of June 8, 1918, upon radiation and other meteorological elements. – Mon. Wea. Rev. **47**, 5–16.

KÖHLER, U., W. VANDERSEE, P. WINKLER, L. GANTNER, 1998: Spectral and integral observations of UV-B-radiation and ozone measurements. – Berichte des DWD **204**, Deutscher Wetterdienst, Offenbach, Germany, 56 pp.

MIMS, F.M. III, E.R. MIMS, 1993: Fluctuations in column ozone during the total solar eclipse of July 11, 1991. – Geophys. Res. Lett. **20**, 367–370.

MÜLLER, M., 1994: Messung der aktinischen ultravioletten Strahlung und der Ozon-Photolysefrequenz in der Atmosphäre mittels Filterradiometrie und Spektralradiometrie. – Dissertation, Rheinische Friedrich-Wilhelms-Universität, Bonn, 196 pp.

NAKAJIMA, T., M. TANAKA, 1988: Algorithms for radiative intensity calculations in moderately thick atmospheres using a truncation approximation. – J. Quant. Spectrosc. Radiat. Trans. **40**, 51–69.

OUTCALT, S.I., D.D. MEISEL, 1970: Micrometeorological observations of a soil surface during the partial phase of the total solar eclipse of March 7, 1970. – Arch. Meteorol. Geophys. Bioklimatol., Ser. B **18**, 287–294.

OSHEROVICH, A.L., N.S. SHPAKOV, V.T. ZARBAYLO, 1974: Measurements of total ozone content during the total solar eclipse of July 11, 1972.– Izv. Atmos. Ocean. Phys. **10**, 755–757.

REUDER, J., 1999: Untersuchungen zur Variabilität von Photolysefrequenzen. – Dissertation, Brandenburgische-Technische-Universität Cottbus, BTUC-AR 4/99, 126 pp.

REUDER, J., T. GORI, L. KINS, R. DLUGI, 1996: Determination of photolysis frequencies of ozone and nitrogen dioxide during SANA2. – Meteorol. Z. **5**, 234–244.

RUGGABER, A., R. DLUGI, T. NAKAJIMA, 1994: Modelling radiation quantities and photolysis frequencies in the troposphere. – J. Atmos. Chem. **18**, 171–210.

SCHWANDER, H., A. KAIFEL, A. RUGGABER, P. KOEPKE, 2001: Spectral radiative-transfer modeling with minimized computation time by use of a neural-network technique. – Appl. Opt. **40**, 331–335.

SCHEFFLER, H., H. ELSÄSSER, 1974: Physik der Sterne und der Sonne. – Bibliographisches Institut, Zürich, 535 pp.

SECKMEYER, G., R. ERB, A. ALBOLD, 1996: Transmittance of a cloud is wavelength dependent in the UV-range. – Geophys. Res. Lett. **23**, 2753–2755.

STRANZ, D., 1961: Ozone measurements during solar eclipse. – Tellus **13**, 276–279.

SVENSSON, B., 1957: Observations on the amount of ozone by Dobson spectrophotometer during the solar eclipse of June 30, 1954. – Arkiv für Geophysik **2**, 573–594.

THIEL, S., 1999: Einfluss von Bewölkung auf die UV-Strahlung an der Erdoberfläche und ihre ökologische Bedeutung. – Dissertation, Berichte des Meteorologischen Institutes der Universität Freiburg, Nr. 3, 231 pp.

U.S. NAVAL OBSERVATORY, 1998: The Astronomical Almanac for the year 1999, 568 pp.

WALDMEIER, M., 1941: Ergebnisse und Probleme der Sonnenforschung. – Probleme der kosmischen Physik, JENSEN, C. (Ed.), Band **22**., Akademische Verlagsgesellschaft Becker & Erler, Leipzig, 264 pp.

WINKLER, P., U. KAMINSKI, U. KÖHLER, J. RIEDL, H. SCHROERS, D. ANWENDER, 2001: Development of meteorological parameters and total ozone during total eclipse of August 11, 1999. – Meteorol. Z. **10**, 193–199.